4

ABSORBING BOUNDARY CONDITIONS FOR THE DIRECT SOLUTION OF PARTIAL DIFFERENTIAL EQUATIONS ARISING IN ELECTROMAGNETIC SCATTERING PROBLEMS

R. Mittra and O. Ramahi

4.1 Introduction

In recent years, there has been an increasing interest [1–6] in the solution of electromagnetic scattering problems via a direct solution of Maxwell's equations using finite mathematics, e.g., the finite difference (FD) and finite element (FEM) techniques, because such a direct formulation of the scattering problem appears to be especially well-suited for scatterers of complex shape and with inhomogeneous coatings. Typically, an integral equation formulation, using the two-dimensional surface current distribution as the unknown and the method of moments (MOM) as the solution procedure, is more efficient

than the partial differential equation schemes for perfectly conducting scatterers because the PDE formulation must work with the electric and magnetic field components at a large number of mesh points in the region surrounding the scatterer. However, this relative advantage of the integral equation schemes narrows for more complex, inhomogeneous scatterers where a three-dimensional, volume type of integral equation must be used. Furthermore, finite methods have an attractive feature–they generate highly sparse and banded matrices which can be efficiently handled using special algorithms. In contrast, the method of moment procedure yields a dense matrix equation that is typically solved using conventional schemes, e.g., the Gaussian elimination method, which is quite time-consuming for large matrices. Thus, PDE formulations have a potential advantage over the integral equation schemes for solving complex, large-body scattering problems.

When solving an open region scattering problem by using finite mathematics approaches, an artificial outer boundary is typically introduced in order to bound the region surrounding the scatterer that is subdivided into meshes for the purpose of discretization. This truncation of the open region enables one to limit the number of unknowns to a manageable size that can be fitted into the computer memory. However, such a truncation also introduces an error and, in order to model the physical problem as correctly as possible, an absorbing boundary condition (ABC) must be imposed on the outer boundary such that it appears as nearly transparent as possible to the waves impinging upon it from the interior. The functions of this absorbing boundary, of course, are to minimize the nonphysical reflections from this boundary and to simulate the condition in which the waves are entirely outgoing as closely as possible. Clearly, in the asymptotic limit where the outer boundary tends to infinity, the absorbing boundary condition should become identical to the Sommerfeld radiation condition. However, in practice, it is desirable to bring in the outer boundary as close to the scatterer as possible in order to reduce the number of mesh points and, hence, the size of the associated matrix. The important question is: How can this be done by enforcing a boundary condition on the outer boundary that suppresses the reflections from it and thus introduces little error in the solution due to truncation of the region external to the scatterer?

Several ABC's , typically in the form of boundary operators, have recently been reported in the literature. These can be broadly classified into two categories, viz., local and nonlocal. In principle, the nonlocal

boundary conditions allow one to bring in the outer boundary as close to the scatterer as desired. However, they have the drawback that they destroy the highly sparse nature that is so characteristic, and distinctly advantageous feature for numerical solution, of the matrices generated via finite methods. These boundary conditions have been discussed by McDonald and Wexler [1] and by MacCamy and Marin [3] and the reader is referred to the above works for additional details.

In contrast, the local boundary conditions yield matrix operators that preserve, at least for the lower-order operators, the highly sparse and banded character of the resulting matrix equations and, hence, do not compromise the computational efficiency of the finite methods. However, not unexpectedly, the local operators are not exact in their modeling of the physical problem, since they are not totally absorbing in nature. As a result, using a local boundary condition introduces some error into the field solution, due primarily to reflections of the outgoing wave from the artificial outer boundary [2,4,5]. The local boundary condition is also inaccurate when traveling waves are excited on the scatterer and substantial global type of coupling exists between widely separated parts of the scatterer.

A number of authors have investigated local ABC's, notably Bayliss, Gunzburger, and Turkel [5], who have employed an asymptotic analysis to derive a series of local operators, referred to henceforth in this paper as the BGT operators. Using the pseudo-differential operator theory, Engquist and Majda [2] have generated a set of different operators which, although not as accurate as the BGT operators, are nonetheless designed to serve the same purpose, viz., a minimization of the reflections from the outer boundary by applying a local form of boundary condition on the fields at this boundary.

In the first part of this work, we begin by briefly reviewing the derivation of the Bayliss, Gunzburger, and Turkel (BGT) boundary operators. Next, we present an alternative approach to deriving the local form of boundary operators and compare the expression obtained from this approach to those based upon the BGT operator. Following this, we carry out a systematic study of the errors resulting from the application of the second and fourth order local operators on an arbitrary scattered field, which can in general be represented in terms of cylindrical harmonics. We do this by comparing the results obtained by using the approximate and the exact boundary conditions, the latter being readily derivable for these harmonics. We show that such an error analysis not only provides a great deal of physical insight into

the mechanism by which the errors are introduced into the process of applying the local operators, but also suggests ways by which a systematic improvement of the ABC-based solution can be achieved. Next, we present the formulation of the ABC in the context of the finite element method (FEM) and provide illustrative numerical results for RCS computation from a number of different geometries.

The question of improvement of the ABC solution is an important one and, to the best of our knowledge, has not been addressed in the past. In this work we provide a systematic procedure based on a hybrid technique that combines the ABC approach with the Unimoment method [7] in a manner that realizes a considerable improvement over that achievable with either of these two individual approaches. A simple but illustrative example of such a procedure is included in the paper as are the results demonstrating the improvement.

The subject of three-dimensional ABC is discussed only briefly in this work, as it is intended to be covered more fully in a forthcoming paper [16]. However, the Appendix does include yet another approach for deriving the two-dimensional ABC based on the use of recursion relations for the expansion coefficients of the asymptotic representation for the field and generalizes it to the three-dimensional scalar and vector cases. Finally, the last section of the paper presents a direct approach for truncating the grid at the outer boundary and indicates how this approach can be conveniently applied to the 3-D vector case. This last approach is based on extrapolating the field using an asymptotic representation, introduced by Wilcox [11], in which the vector EM fields are expressed in terms of a series of inverse powers in r, the radial distance from the origin.

4.2 Derivation of the BGT Operators

In this section we briefly review the derivation of the BGT type of absorbing boundary condition by considering the example of a two-dimensional, perfectly-conducting scatterer. The conclusions, however, apply to general scatterers that may be combinations of p.e.c's (perfect electric conductors) and/or inhomogeneous dielectrics.

Consider a perfectly conducting cylindrical scatterer, shown in Fig. 1, whose cross-section is defined by the contour Γ_1. Let the exterior region of the scatterer be designated by the domain Ω. For a TM-polarized incident wave, the problem at hand is to solve the wave equation

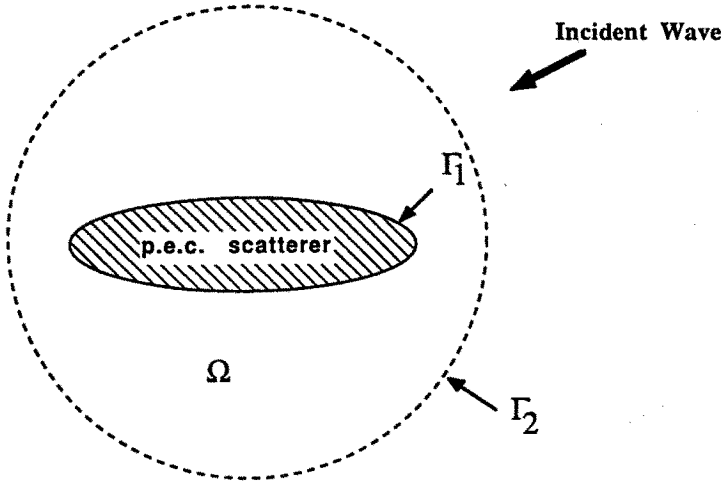

Figure 1 Geometry for the finite-mathematics approach to the scattering problem.

$$\nabla^2 u + k^2 u = 0 \tag{1}$$

where the wave function u is proportional to the z-component of the scattered electric field. The wave function satisfies the boundary condition

$$u^i + u = 0 \text{ on } \Gamma_1 \tag{2}$$

where u^i is the incident wave function .

Following Wilcox, an asymptotic expression for u can be written at large distances from the origin as follows:

$$u \approx \frac{e^{-jk\rho}}{\sqrt{\rho}} \left[a_0(\phi) + \frac{a_1(\phi)}{\rho} + \frac{a_2(\phi)}{\rho^2} + \ldots \right] \tag{3}$$

Defining u_ρ as the ρ derivative of u, we have, from (3),

$$u_\rho + jku = -\frac{e^{-jk\rho}}{2\rho^{3/2}} \left[a_0(\phi) + 3\frac{a_1(\phi)}{\rho} + 5\frac{a_2(\phi)}{\rho^2} + \ldots \right] \tag{4}$$

From (4), we obtain

$$(u_\rho + \jmath k u) = O\left[\frac{1}{\rho^{3/2}}\right] \tag{5}$$

From (5), we note that if we neglect terms on the order of $O(\rho^{-3/2})$ and smaller, we obtain $u_\rho + \jmath k u = 0$, which is precisely equivalent to the Sommerfeld radiation condition for u in two dimensions. Next, we show that we can obtain a higher-order boundary operator B_1, shown below, that yields terms on the order of $O(\rho^{-5/2})$ when applied to the wave function u. The operator B_1 is given by

$$B_1 = \frac{\partial}{\partial \rho} + \jmath k + \frac{1}{2\rho} \tag{6}$$

and we readily find that, for a given ρ, B_1 introduces a higher-order (in ρ^{-1}) error than does the Sommerfeld radiation condition, since

$$B_1 u = u_\rho + \jmath k u + \frac{1}{2\rho} u = O\left[\frac{1}{\rho^{5/2}}\right] \tag{7}$$

Continuing along similar lines, the next higher-order operator B_2 can be derived by first defining $v = B_1 u$, and then showing that

$$\left(\frac{\partial}{\partial \rho} + \jmath k + \frac{5}{2\rho}\right) v = O(\rho^{-9/2})$$

Thus, if we define

$$B_2 = \left(\frac{\partial}{\partial \rho} + \jmath k + \frac{5}{2\rho}\right)\left(\frac{\partial}{\partial \rho} + \jmath k + \frac{1}{2\rho}\right)$$

we see that

$$B_2 u = B_1 v = \left[\frac{\partial}{\partial \rho} + \jmath k + \frac{5}{2\rho}\right]\left[\frac{\partial}{\partial \rho} + \jmath k + \frac{1}{2\rho}\right] u = O\left[\frac{1}{\rho^{9/2}}\right] \tag{8}$$

Bayliss et al. have shown that a generalized operator B_m can be constructed by repeating the above procedure, where

$$B_m = \prod_{p=1}^{m}\left[\frac{\partial}{\partial \rho} + \frac{2\rho - 3/2}{\rho} + \jmath k\right] \tag{9}$$

and

$$B_m u = O\left[\frac{1}{\rho^{2m+1/2}}\right] \tag{10}$$

Returning now to the PDE (1), we note that to solve it using the finite mathematics methods, the differential equation or its variational form must be discretized in a bounded region surrounding the scatterer. Let Γ_2 be the outer boundary where the ABC will be imposed using an m-th order boundary operator. Then for the case where u satisfies the boundary condition on the scatterer that the total $u = 0$, a complete statement of the approximated scattering problem in the bounded region reads

$$\nabla^2 u + k^2 u = 0 \quad \text{in } \Omega$$

$$u^i + u = 0 \quad \text{on } \Gamma_1$$

$$B_m u = 0 \quad \text{on } \Gamma_2 \tag{11}$$

Equation (11) can now be solved for u using the FD or FEM schemes and the field in region Ω as well as the scattered far field can be computed. If the solution obtained using a certain boundary operator B_n is not sufficiently accurate, then one has the option of either receding Γ_2 farther away from the scatterer, or employing higher-order boundary operators. However, the boundary operators with $n > 2$ are typically not recommended for numerical implementation because they spoil the sparsity of the matrix. It should also be noted that the boundary operators are asymptotic in nature and, consequently, using higher-order operators may not necessarily ensure a continued improvement of the solution when the outer boundary Γ_2 is close to the surface of the scatterer. Finally, even though according to (10) the estimate of the error in $B_n u$ is $O(1/\rho^{(2n+1/2)})$, the actual error in u may be substantially different from the estimated error in $B_n u$ given by (10). For instance, for the numerical example given in section 4 where B_2 is used to derive the solution to the problem of catering by a conducting cylinder of radius $ka = 50$, it is found that the maximum error in u on the boundary is approximately 20% of the incident field, i.e., about eight orders of magnitude greater than $(k\rho)^{-9/2}$ for $k\rho = 51$. Furthermore, it should be realized that the use of the n-th order ABC with a finite

n introduces reflections from the outer boundary and, hence, the solution generated using this boundary condition does not strictly satisfy the Wilcox-type representation (3) containing outgoing waves only.

4.3 Alternate Boundary Condition for 2-D Scattering

In this section, we present an alternate derivation of the boundary operators by postulating the higher-order radiation condition for u in the form of an asymptotic series in inverse powers of ρ with unknown coefficients, substituting this form into the differential equation,and systematically solving for the coefficients of the series representation for the extended radiation condition, or ABC. We begin with the following representation for u_ρ for large ρ, which contains higher order angular derivatives in ϕ, and not in ρ as in (8) or (10), and is found to be better-suited for numerical implementation

$$u_\rho \approx \alpha(\rho)u + \beta(\rho)\, u_{\phi\phi} \tag{12}$$

and write both α and β in the form of asymptotic series

$$\alpha(\rho) = \alpha_0 + \frac{\alpha_1}{\rho} + \frac{\alpha_2}{\rho^2} + \frac{\alpha_3}{\rho^3} \tag{13}$$

$$\beta(\rho) = \beta_0 + \frac{\beta_1}{\rho} + \frac{\beta_2}{\rho^2} + \frac{\beta_3}{\rho^3} \tag{14}$$

We now show that the unknown coefficients $\alpha(\rho)$ and $\beta(\rho)$, or more specifically α_n and β_n, can be systematically found via recursion relations. To this end, we substitute u_ρ, given in (12), into the wave equation (1). This yields

$$\left[\frac{\alpha}{\rho} + \alpha_\rho + \alpha^2 + k^2\right] u + \left[\frac{\beta}{\rho} + 2\alpha\beta + \beta_\rho + \frac{1}{\rho^2}\right] u_{\phi\phi} = 0 \tag{15}$$

where the fourth-order angular derivative $u_{\phi\phi\phi\phi}$ has been neglected for the purpose of deriving the second-order ABC operator. Since (15) is valid for an arbitrary ρ, the coefficients of u and $u_{\phi\phi}$ must be individually zero. Thus, we must have

$$\frac{\alpha}{\rho} + \alpha_\rho + \alpha^2 + k^2 = 0 \tag{16}$$

and

$$\frac{\beta}{\rho} + 2\alpha\beta + \beta_\rho + \frac{1}{\rho^2} = 0 \tag{17}$$

Substituting $\alpha(\rho)$ into (16), we obtain

$$(\alpha_0^2 + k^2) + (\alpha_0 + 2\alpha_0\alpha_1)\frac{1}{\rho} + (\alpha_1^2 + 2\alpha_0\alpha_2)\frac{1}{\rho^2}$$

$$+ (2\alpha_0\alpha_3 + 2\alpha_1\alpha_2 - \alpha_2)\frac{1}{\rho^3} + O\left[\frac{1}{\rho^4}\right] = 0 \tag{18}$$

Equating the coefficients of ρ^{-n} to 0, we have

$$\alpha_0^2 + k^2 = 0 \tag{19}$$

$$\alpha_0 + 2\alpha_0\alpha_1 = 0 \tag{20}$$

from which we can recursively derive

$$\alpha_0 = -\jmath k$$

$$\alpha_1 = -\frac{1}{2}$$

$$\alpha_2 = -\frac{\jmath}{8k}$$

$$\alpha_3 = \frac{1}{8k^2} \tag{21}$$

Thus, we can write

$$\alpha = \left[-\jmath k - \frac{1}{2\rho} - \frac{\jmath}{8k\rho^2} + \frac{1}{8k^2\rho^3}\right] \tag{22}$$

Substituting $\beta(\rho)$ into (17) and following the same procedure as outlined above, we obtain

$$\beta = \left[\frac{-\jmath}{2k\rho^2} + \frac{1}{2k^2\rho^3}\right] \tag{23}$$

Using the above expressions for α and β in (12), we obtain the second-order boundary operator $\mathcal{B}_2$

$$\mathcal{B}_2 u = u_\rho - \alpha(\rho)u - \beta(\rho)U_{\phi\phi} \tag{24}$$

We can also rewrite the B_2 operator, given in (8) as

$$B_2 u = u_\rho - \left[\frac{1}{1-\frac{\jmath}{k\rho}}\right] \cdot \left\{\left[-\jmath k - \frac{3}{2\rho} + \frac{3\jmath}{8k\rho^2}\right] u + \left[\frac{-\jmath}{2k\rho^2}\right] u_{\phi\phi}\right\} \tag{25}$$

where we have used (1) to trade the second order radial derivative with the second order angular derivative, the latter being better suited for numerical implementation. By expanding the coefficients of u and $u_{\phi\phi}$ in (25) and retaining terms up to order ρ^{-3}, we obtain

$$B_2 u = u_\rho - \left[-\jmath k - \frac{1}{2\rho} - \frac{\jmath}{8k\rho^2} + \frac{1}{8k^2\rho^3}\right] u + \left[\frac{-\jmath}{2k\rho^2} + \frac{1}{2k^2\rho^3}\right] u_{\phi\phi} \tag{26}$$

We observe by comparison of (24) and (26), that the second order BGT operator is identical to $\mathcal{B}_2$, up to the order ρ^{-3} retained in $\alpha(\rho)$ and $\beta(\rho)$.

We can follow the procedure outlined above for the derivation of $\mathcal{B}_2$ to obtain higher order boundary operators that involve higher order angular derivatives. Following an analogous development, we represent higher order operators in the form

$$u_\rho = \alpha(\rho)u + \beta(\rho)u_{\phi\phi} + \gamma(\rho)u_{\phi\phi\phi} + \delta(\rho)u_{\phi\phi\phi\phi} + \ldots \tag{27}$$

where the radially dependent coefficients, α, β, γ and δ, can be found by following the same procedure used to derive the coefficients of the $\mathcal{B}_2$ operator. One finds that γ, the coefficient of $u_{\phi\phi\phi}$, must be zero in order for the above form in (27) to satisfy the Helmholtz equation in (1). Thus, the next higher order operator after $\mathcal{B}_2$ will have the fourth angular derivative in u instead of the third. Consequently, we designate this operator as $\mathcal{B}_4$ which is given by

$$\mathcal{B}_4 u = u_\rho - \alpha(\rho)u - \beta(\rho)u_{\phi\phi} - \delta(\rho)u_{\phi\phi\phi\phi} \tag{28}$$

where $\alpha(\rho)$ and $\beta(\rho)$ are the same (within ρ^{-3}) as in (22) and (23) respectively, and $\delta(\rho)$ is given by

$$\delta(\rho) = \frac{j}{8k^3\rho^4} \tag{29}$$

In the next section we present comparative results for the two operators $\mathcal{B}_2$ and $\mathcal{B}_4$. Of course, it is evident that they both reduce to the Sommerfeld radiation condition when the outer boundary is placed sufficiently far away from the scatterer.

Before closing this section, we mention that an even more direct derivation of the $\mathcal{B}_2$ and $\mathcal{B}_4$ operators is possible by using the recursion relationship satisfied by coefficients $a_n(\phi)$ of ρ^{-n} appearing in the Wilcox-type expansion (3). This is shown in the Appendix, where the ABC's for three-dimensional scalar and vector wave functions, derived by using appropriate recursion relationships valid for the coefficients for the 3-D type of Wilcox's expansion, are also given for reference.

4.4 Performance of Boundary Operators

Typically, to assess the accuracy of the local boundary operators discussed above, one would apply these operators to the outer boundary, construct the field solution using one of the finite mathematics methods, and compare the results for the surface current, the far field, the radar cross section, etc., with those obtained using an alternate approach, e.g., the moment method or experimental measurements. However, in this paper we present a numerical comparison of the results of the application of the $\mathcal{B}_2$ and $\mathcal{B}_4$ operators on an arbitrary scattered field represented in terms of cylindrical harmonics, taking advantage of the fact that an exact boundary condition can be found for these harmonics. We show that such a comparison reveals a great deal of insight into the behavior of the local boundary operators, explains why they fail when they do, and provides a clue as to how the approximate numerical results obtained via the application of the second-order boundary operators can systematically be improved. It is well known that external to a cylindrical region circumscribing an arbitrary scatterer, the wave function u representing the scattered field can always be expressed as

$$u = \sum_{n=-N}^{N} a_n H_n^{(2)}(k\rho) e^{jn\phi} \tag{30}$$

Obviously, the representation above not only satisfies the radiation condition at infinity but is also outgoing for all values of ρ. To determine the sort of error that is introduced when we apply the second-order boundary operator (which we know satisfies the outgoing condition only approximately) to this representation, we substitute the representation for u in (30) into the boundary operator to obtain

$$u_\rho^{\text{exact}} = \sum_{n=-N}^{N} a_n \frac{\partial H_n^{(2)}(k\rho)}{\partial \rho} e^{jn\phi} \tag{31a}$$

From (27) we have

$$\begin{aligned} u_\rho^{\text{approx}} = \alpha(\rho) &\sum_{n=-N}^{N} a_n H_n^{(2)}(k\rho) e^{jn\phi} \\ -\beta(\rho) &\sum_{n=-N}^{N} a_n H_n^{(2)}(k\rho) n^2 e^{jn\phi} \\ +\delta(\rho) &\sum_{n=-N}^{N} a_n H_n^{(2)}(k\rho) n^4 e^{jn\phi} \end{aligned} \tag{31b}$$

Using the separability in ϕ, we obtain the error, E_n, in the n-th harmonic content of u_ρ as

$$E_n = \frac{\partial H_n^{(2)}(k\rho)}{\partial \rho} - [\alpha(\rho) - n^2\beta(\rho) + n^4\delta(\rho)] H_n^{(2)}(k\rho) \tag{32}$$

where

$$\begin{aligned} \alpha(\rho) &= -jk - \frac{1}{2\rho} - \frac{j}{8k\rho^2} + \frac{1}{8k^2\rho^3} \\ \beta(\rho) &= -\frac{j}{2k\rho^2} + \frac{1}{2k^2\rho^3} \end{aligned} \tag{33}$$

and

$$\delta(\rho) = \begin{cases} \dfrac{j}{8k^3\rho^4} & \text{for } \mathcal{B}_4 \\ 0 & \text{for } \mathcal{B}_2 \end{cases} \tag{34}$$

A convenient way to estimate the error is to compare the two quantities $\gamma_n = H_n'/H_n$ = exact γ_n, with $\gamma_n^{(2)ap} = \alpha(\rho) - n^2\beta(\rho) =$ approximate $\gamma_n^{(2)}$, obtained from the second-order boundary operator, and $\gamma_n^{(4)ap} = \alpha(\rho) - n^2\beta(\rho) + n^4\delta(\rho)$. The quantity γ_n can be physically interpreted to be playing the role of the complex propagation constant for cylindrical fields, since it equals u_ρ/u. We also note that γ_n equals $-jk$ in the far field where u satisfies the Sommerfeld radiation condition.

Figure 2 shows γ_n^{ap}'s calculated at $k\rho = 51$ using the $\mathcal{B}_2$ and $\mathcal{B}_4$ operators and compares them with the corresponding exact γ_n. From Fig. 2a, the imaginary part of γ_n computed by using the $\mathcal{B}_4$ operator is seen to be somewhat superior than the corresponding result derived from the $\mathcal{B}_2$ operator. However, the real part of γ_n^{ap}, which is shown in Fig. 2b, and which dominates when n is large, is seen to differ considerably from the exact γ_n for both. These figures clearly show that the error introduced by the boundary operators is not uniform for all harmonics. It is evident that the boundary operators work quite well for the lower-order harmonics, in that they yield results for γ_n^{ap} that compare very favorably with the exact $\gamma_n = u_\rho/u$ for the outgoing harmonics. The situation changes, however, for the higher-order harmonics, particularly for $n = 40$ on up, where they transition from being essentially propagating (γ_n essentially imaginary), into the evanescent region in which the exact γ_n acquires a significant real part. We note that the approximate γ_n's fail to predict this phenomenon correctly.

As a rule of thumb, to compute the scattered field at $\rho \geq ka$ for a scatterer of characteristic dimension ka, defined as the radius of the smallest circle that encloses the scatterer, the upper limit N for the series in (30) has to be set at least equal to M, where M is slightly larger than ka. Thus, suppose we have a scatterer whose characteristic dimension is given by $ka = 50$, and in an attempt to drastically reduce the number of mesh points, we impose the second-order boundary operator on a circle whose radius is either equal to or only slightly greater than 50. We should expect errors to be introduced into the satisfaction

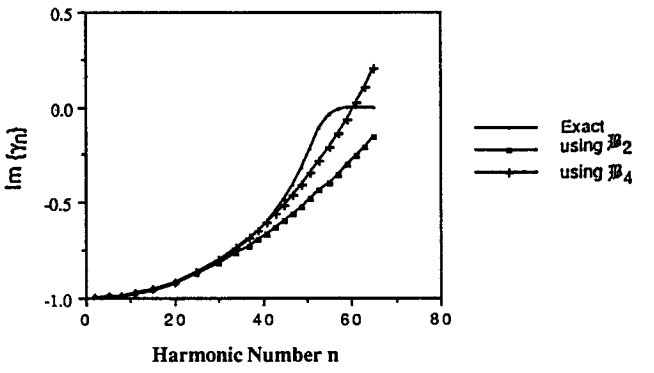

(a)

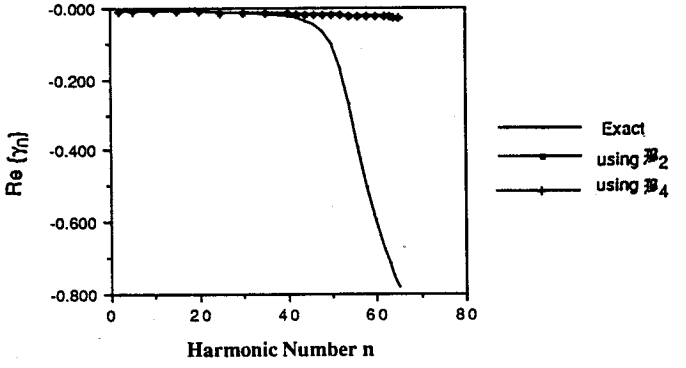

(b)

Figure 2 γ_n **as calculated using the** $\mathcal{B}_2$ **and** $\mathcal{B}_4$ **operators, and the exact** γ_n **at** kb **=51 (a) Imag(γ_n); (b) Real(γ_n).**

of the outgoing type of boundary condition by the harmonic contents of the scattered field falling in the range $40 < n < 60$, that are essentially evanescent or in the transition region. This result provides us with the clue as to why the On-Surface Radiation Condition (OSRC) [12] is expected to work well only for a smooth, moderate-sized scatterer whose scattered field has a relatively low content of higher-order harmonics. It also predicts that when the ABC is applied on or close to the surface of a scatterer that generates a substantial amount of higher-order evanescent harmonics, e.g., a strip, it is likely to introduce significant

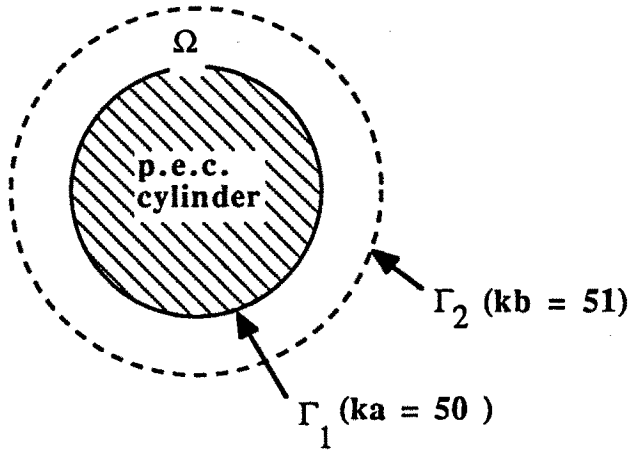

Figure 3 Geometry of p.e.c. cylinder of size $ka = 50$ and artificial boundary at $kb = 51$.

errors in the solution(see for instance [12]). Furthermore, an understanding of the physics of the behavior of higher-order harmonics is also helpful in developing methods by which the solution derived by applying the second-order boundary operator on a surface that is close to the scatterer can be significantly improved. In the following, we first illustrate the principles for implementing such improvement by considering the canonical problem of scattering by a circular cylinder. Next, we consider the case of a general scatterer and indicate how the same concept can be extended to this case.

Consider the problem of TM scattering ($\overline{E}$ parallel to the axis of the cylinder) from a perfectly conducting circular cylinder of radius $ka = 50$, as is illustrated in Fig. 3. We introduce an artificial outer boundary Γ_2 at $k\rho = 51$ and apply the second-order boundary operator $\mathcal{B}_2$ to the scattered field at this boundary. For this canonical problem, the resulting field problem can be solved analytically, and the solution for the scattered far field is shown in Fig. 4. Since we expect reflections from the outer boundary due to the application of the inexact boundary condition at Γ_2, we write the wave function u in the annular region Ω as a sum of outgoing and incoming harmonics, whose weight coefficients

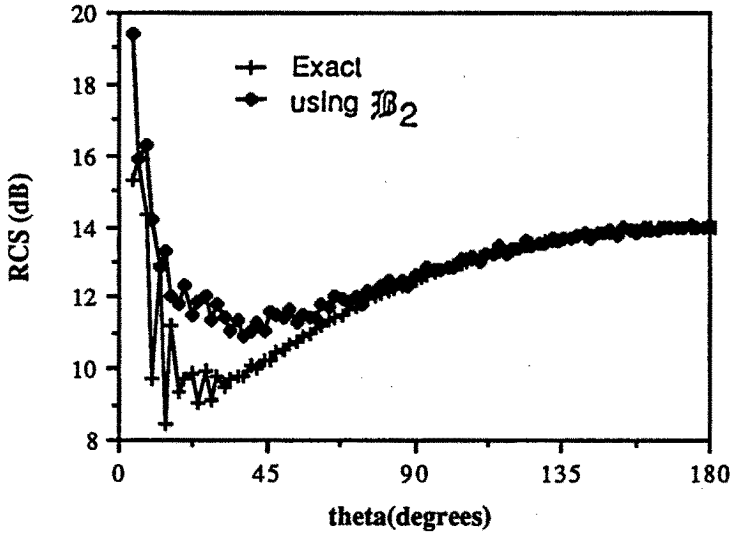

Figure 4 Comparison of exact bistatic RCS with that calculated using the ABC.

are given by a_n and b_n as follows

$$u = \sum_{n=-N}^{N} [a_n H_n^{(2)}(k\rho) + b_n H_n^{(1)}(k\rho)]\, e^{jn\phi} \tag{35}$$

Figures 5 and 6, which plot the incoming and outgoing coefficients, show that the higher-order harmonics generated by using the boundary operator are in error. Referring to Fig. 5, we see that the incoming harmonic coefficients b_n's, which should ideally be identically zero, are not negligibly small for $n > 45$. We also note that, for this example, they are slightly smaller for $\mathcal{B}_4$ than they are for $\mathcal{B}_2$. As for the outgoing harmonics a_n's, shown in Fig. 6, we note that the approximate solutions derived by using the ABC operators also deviate from the exact solution for the higher-order harmonics beyond $n > 45$.

The maximum error in the scattered field u computed by using the ABC is also a quantity of interest and, on the outer boundary located at $k\rho = 51$, this error is found to be 20.5 percent (normalized to the incident field) for $\mathcal{B}_2$ and 12.9 percent for $\mathcal{B}_4$. This is in spite of the fact that, according to (10), the error in the second order operator $\mathcal{B}_2$ was estimated to be on the order of 10^{-8}, and the estimate for the fourth order operator was considerably smaller than that. The reason

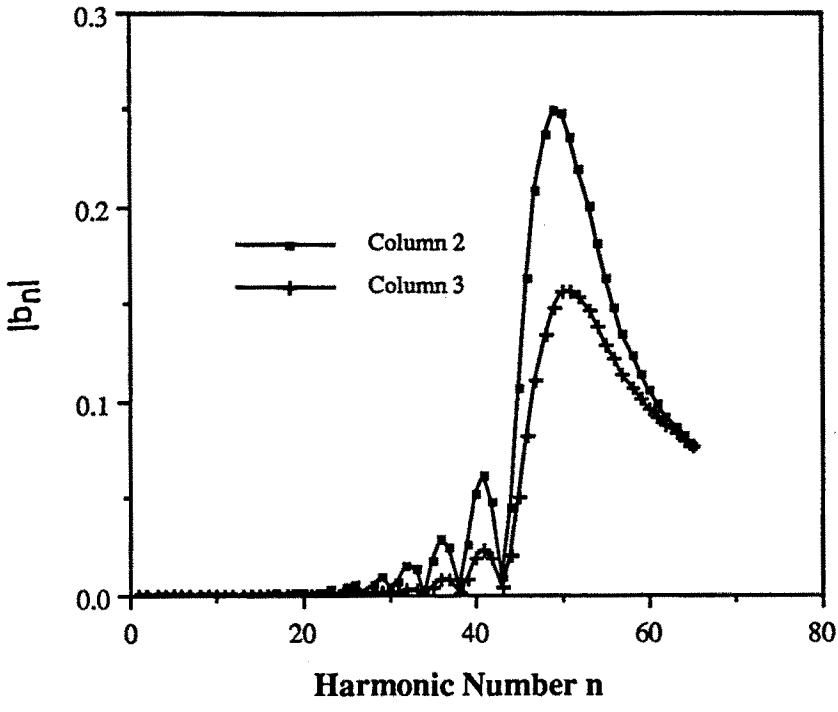

Figure 5 Magnitude of the coefficients of the incoming harmonics, $|b_n|$, as generated by using the ABC.

for this discrepancy can be readily explained if one recognizes that the error terms in the expression for $B_n u$ are dependent not only on the radius of the outer boundary, but also on the shape of the scatterer as well as the nature of the incident field. Specifically, the coefficient of the $\rho^{-9/2}$ term in the expression for $B_2 u$ may be quite large (on the order of 10^7 for the present problem) and, consequently, an error prediction based solely on the radius of the outer boundary where the ABC is applied may be substantially inaccurate.

Although, thus far we have only presented some representative results for the TM-case in this paper, we have also carried out similar calculations for the TE case and have found that, in general, the ABC approach works less well for this case than it does for the TM-polarized incident field. This will be evident from some of the results appearing in the next section where we discuss the implementation of the absorbing boundary condition in the context of the FEM formulation.

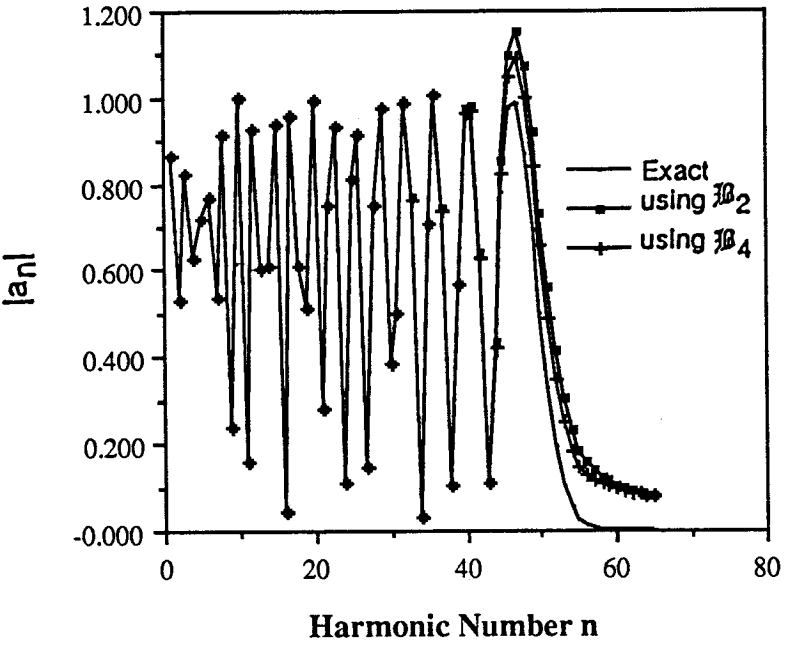

Figure 6 Magnitude of the coefficients of the outgoing harmonics, $|a_n|$, generated by using the ABC and compared with the exact $|a_n|$.

4.5 Absorbing Boundary Condition for the FEM

In this section, we describe the implementation of the ABC into the finite-element formulation, which is used very frequently in PDE approaches to solving scattering problems from complex targets. Detailed account of the finite-element method can be readily found in the existing literature (see for instance [13–15]) and, hence, only a brief summary of the governing equations are included here.

We return to (1), the wave equation satisfied by the scattered field and rewrite it below for convenience

$$\nabla^2 u + k^2 u = 0 \tag{36}$$

The first step in the FEM formulation is to multiply the above Helmholtz equation with a test function v, and integrate the product over the domain of the problem, viz., Ω (see Fig. 1). This gives

$$\int_{\Omega_1} (v\nabla^2 u + k^2 vu)\, ds = 0 \tag{37}$$

The second step involves transferring the differentiation from the unknown function u to the testing function v via the Green's identity as follows

$$\int_{\Omega} v\,\nabla^2 u\, ds = -\int_{\Omega} \nabla u \cdot \nabla v\, ds + \int_{\Gamma_1+\Gamma_2} v\,\frac{\partial u}{\partial n}\, dl \tag{38}$$

Substituting this identity into the variational from in (36), we arrive at the weak form of the Helmholtz equation

$$\int_{\Omega} (\nabla u \cdot \nabla v - k^2 vu)\, ds = \int_{\Gamma_1+\Gamma_2} v\,\frac{\partial u}{\partial n}\, dl \tag{39}$$

where Γ_1 and Γ_2 describe the boundary of the solution region as shown in Fig. 1. Finally, the absorbing boundary condition is incorporated into the weak form by inserting the B_2 operator into the right hand side integral over Γ_2, which is the outer boundary contour. This gives

$$\int_{\Omega} (\nabla u \cdot \nabla v - k^2 vu)\, ds = \int_{\Gamma_1} v\,\frac{\partial u}{\partial n}\, dl + \int_{\Gamma_2} v\,(\alpha u + \beta u_{\phi\phi})\, dl \tag{40}$$

Integrating the term in the integrand involving $u_{\phi\phi}$ by parts, and introducing a change of variables, we get

$$\int_{\Omega} (\nabla u \cdot \nabla v - k^2 vu)\, ds = \int_{\Gamma_1} v\,\frac{\partial u}{\partial n}\, dl + \int_{\Gamma_2} (\alpha vu - \beta\rho^2 v_l\, u_l)\, dl \tag{41}$$

where v_l and u_l are the tangential derivatives along the outer contour Γ_2.

The form given in (41) is well-suited for numerical implementation, especially if first order finite elements are chosen to discretize the region Ω. Notice that if the ABC operator, e.g., B_4, were used in place of the B_2 operator employed above, second or higher-order angular derivatives would have appeared in the boundary integral. This would, in turn, have necessitated the use of second or higher order elements, and, consequently, would have resulted in decreased sparsity of the system matrix.

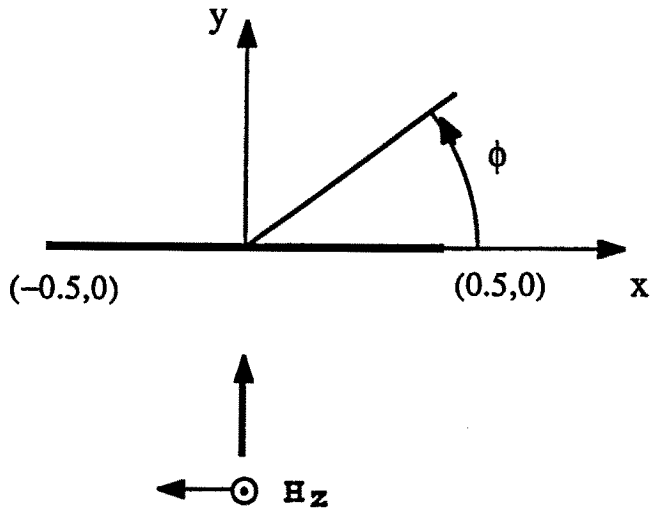

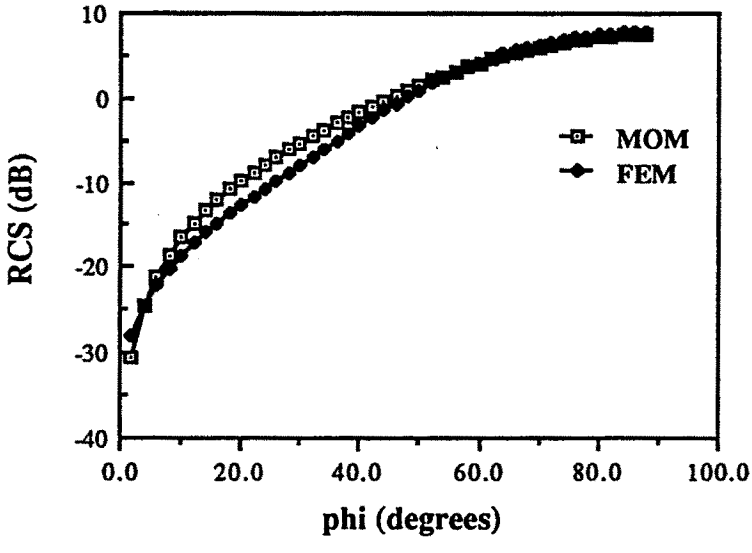

Figure 7 Bistatic radar cross section of a conducting strip, TE case, computed by using the ABC method with $\mathcal{B}_2$ operator applied at 1.1λ.

For the TM-polarization case, we have $u = E_z$, and since the field values are specified on the surface of the scatterer, there is no boundary-integral contribution from Γ_1 . For the TE-polarization,

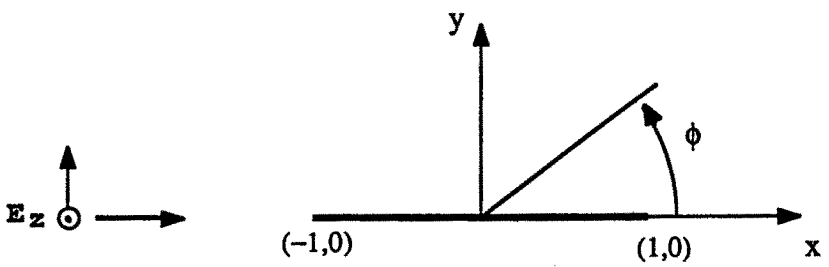

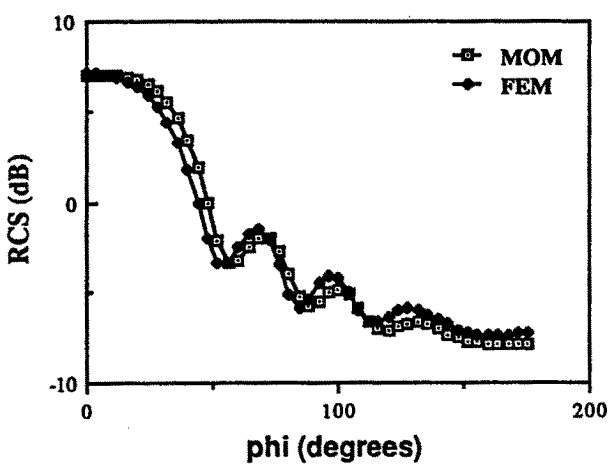

Figure 8 Bistatic radar cross section of a conducting strip, TM case, computed by using the ABC method with $\mathcal{B}_2$ operator applied at 1.2λ.

$u = H_z$, and the boundary condition on the p.e.c. cylinder is given by

$$\left[\frac{\partial u}{\partial n} + \frac{\partial u^{\text{inc}}}{\partial n}\right] = 0 \tag{42}$$

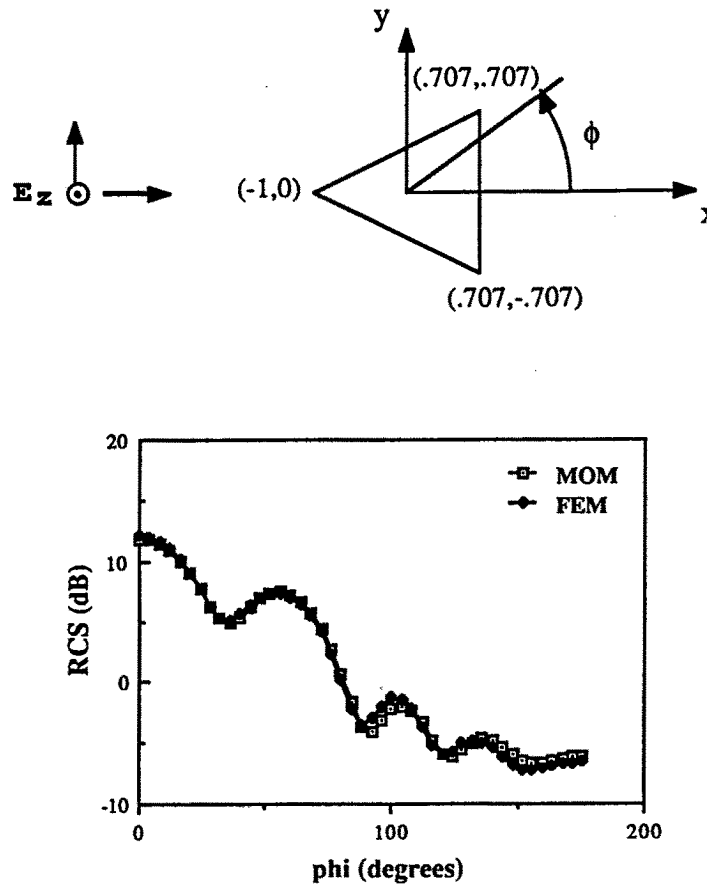

Figure 9 Bistatic radar cross section of a conducting triangular cylinder, TM case, computed by using the ABC method with $\mathcal{B}_2$ operator applied at 1.3λ.

This condition is substituted in the boundary integral over Γ_1 for the TE polarization. However, the condition on the outer boundary, viz., Γ_2, remains the same for both polarizations.

Numerical results for RCS computation from several representative structures will now be presented. The geometries considered are a 1λ strip, a triangular cylinder, and two circular cylinder geometries

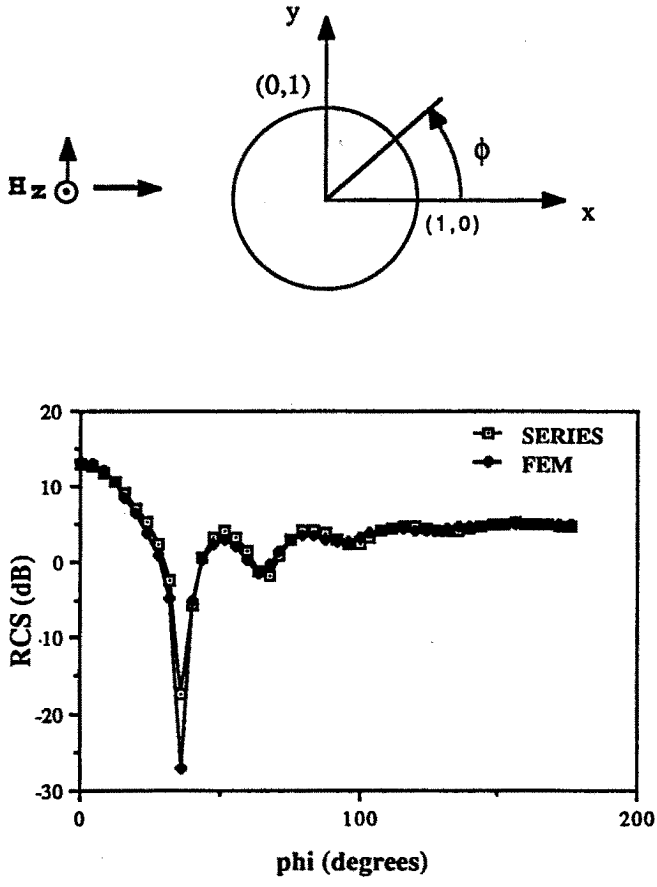

Figure 10 Bistatic radar cross section of a conducting circular cylinder, TE case, computed by using the ABC method with $\mathcal{B}_2$ operator applied at 1.1λ.

of radii 1λ and 8λ, respectively. The bistatic radar cross sections of these scatterers are shown in Figs. 7 through 12, where they are also compared with the results derived from other available techniques e.g., the method of moments and the series solution for circular cylinders. It is evident from these results that for small scatterers the ABC approach yields results that are in excellent agreement with the method

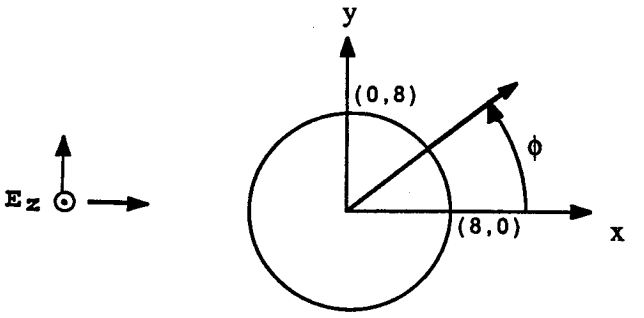

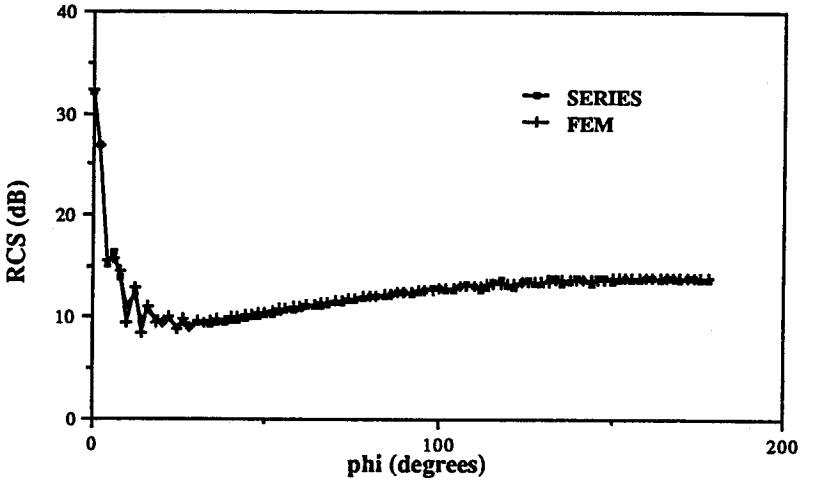

Figure 11 Bistatic radar cross section of a conducting circular cylinder of radius 8λ, TM case, computed by using the ABC method with $\mathcal{B}_2$ operator applied at 8.2λ.

of moments, regardless of the polarization of the incident field. For larger scatterers, it is found that the ABC approach continues to work reasonably well for the TM polarization, as is evident from the example of Fig. 11 for a cylinder of radius 8λ. For TE polarization the ABC deteriorates more rapidly and the errors in the solution show up sooner than they do for the TM case, i.e., for smaller body sizes in terms of

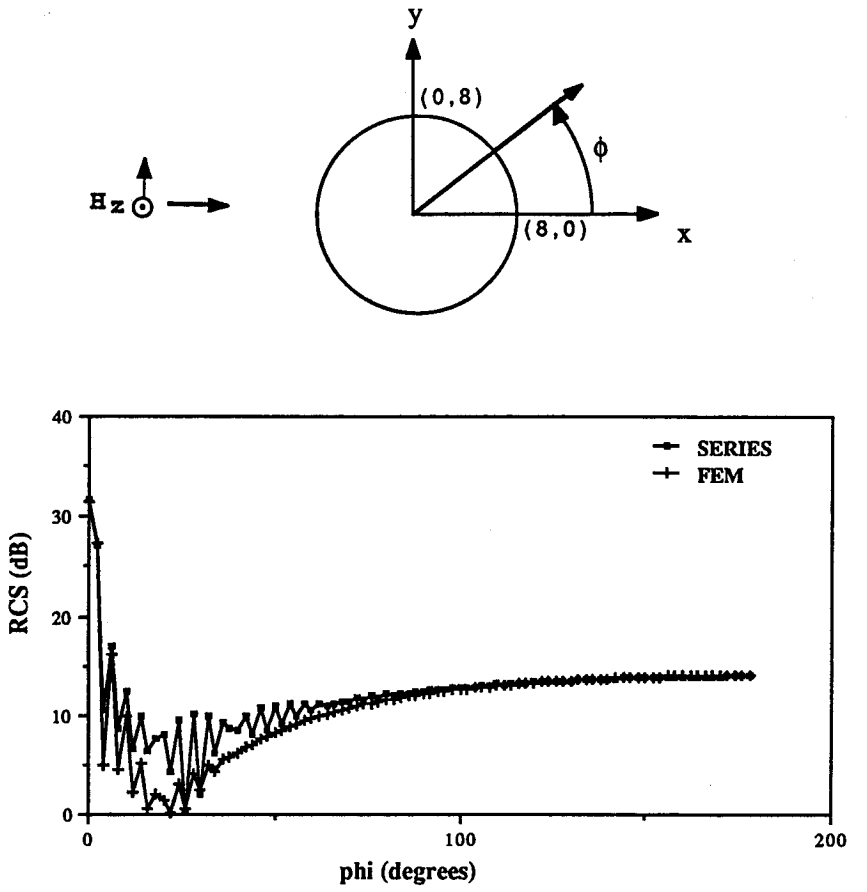

Figure 12 Bistatic radar cross section of a conducting circular cylinder of radius 8λ, TE case, computed by using the ABC method with $\mathcal{B}_2$ operator applied at 8.2λ.

ka. We see, for instance, from Figs. 11 and 12, that the results for the 8λ cylinder are less accurate for the TE case than they are for the comparable TM case.

4.6 Improvement in the ABC-Based Solution

As a first step toward improving the ABC-based solution, we might attempt to purify the approximate solution by filtering out all of the incoming harmonic contributions and using only the outgoing harmonics to compute the far scattered fields. This can always be done, in general, even for an arbitrary scatterer, by starting with the computed values of u and u_ρ on the outer boundary $\rho = b$, Fourier analyzing these values to determine the coefficients of the incoming and outgoing harmonics and, deleting the incoming harmonics while retaining the outgoing ones with their coefficients intact. While this procedure is simple, and would in general yield a better solution for the far field, it can be further refined by recognizing that that the coefficients of the outgoing harmonics are still in error and should be corrected for improved accuracy.

To achieve improvement in the result beyond that obtainable via the simple deletion of the incoming harmonics, we must attempt to annihilate, or at least minimize, the coefficients of the higher-order incoming harmonics that are significant while *simultaneously* adjusting the outgoing harmonic coefficients associated with the same harmonics. The procedure followed for this test problem is explicitly outlined below.

By enforcing the boundary condition on the perfect electric conductor at ka and applying the boundary operator at kb, we obtain the matrix equation

$$\begin{bmatrix} H_n^{(1)}(ka) & H_n^{(2)}(ka) \\ H_n^{(1)}(kb) & H_n^{(2)}(kb) \end{bmatrix} \begin{bmatrix} b_n \\ a_n \end{bmatrix} = \begin{bmatrix} -\jmath^{-n} J_n(ka) \\ (a_n + \eta_n) H_n^{(2)}(kb) \end{bmatrix} \tag{43}$$

where η_n's are the corrections in the coefficients of the outgoing harmonics a_n, and are to be determined by imposing the condition that $b_n = 0$. Letting $b_n = 0$, we get

$$(a_n + \eta_n) = \frac{-\jmath^{-n} J_n(ka)}{H_n^{(2)}(ka)} \tag{44}$$

$$\eta_n = \left[\frac{-\jmath^{-n} J_n(ka)}{H_n^{(2)}(ka)} - a_n \right] \tag{45}$$

In Fig. 4, we presented the exact as well as the approximate bistatic RCS, the latter having been calculated using the second-order

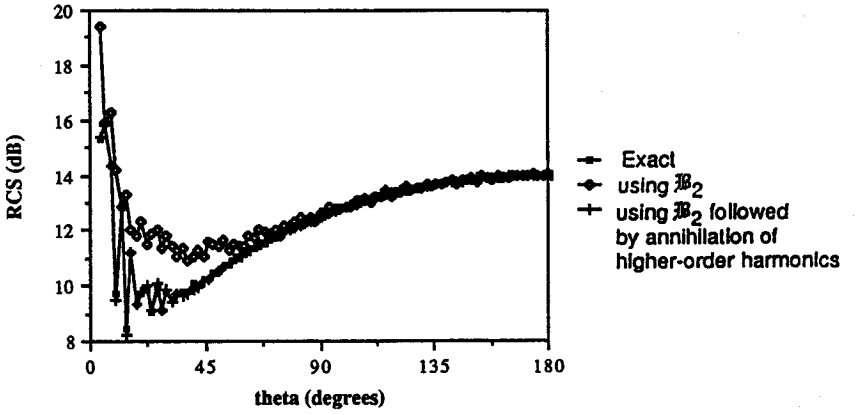

Figure 13 Effect of annihilating the harmonics n=40 through 60 in the ABC solution on the scattered field.

boundary operator $\mathcal{B}_2$, by filtering out the incoming harmonics and retaining only the outgoing ones. We note, first of all, that the RCS results are quite accurate in the forward scatter and backscatter directions, and in the vicinity of these angles, but they do deviate from the true results at other angles. Figure 13 shows the effect of annihilating the higher-order incoming harmonics ranging from $n = 40$ to 60, while simultaneously adjusting the coefficients of the corresponding outgoing harmonics. It is evident that a significant improvement is obtained at the angles where the far field, computed by using the the original $\mathcal{B}_2$ solution and retaining only the outgoing waves without further modification, was in error.

For the canonical problem of a circular cylinder, it was possible for us to systematically improve, by analytical means, the approximate results for the scattered field obtained via the application of the second-order ABC. Obviously, we would expect to have to resort to numerical means when the scatterer is of arbitrary shape. In the following, we indicate how an approach that embodies the concepts of the Unimoment method developed by Mei and his co-workers [7–9], can be employed to improve the ABC-based solution for an arbitrary scatterer in a numerically efficient manner.

The first step in the application of the Unimoment method is to enclose the scatterer with an artificial boundary which is separable in

nature, e.g., a circular boundary for the two-dimensional scattering problem. This step not only allows one to conveniently express the solution for the scattered field in the external region in terms of cylindrical wave functions, but it also decouples the exterior problem from the interior one except, of course, via the continuity conditions on the tangential fields to be imposed at the common boundary. Next, one solves the interior problem N times, where N is the number of cylindrical harmonics needed to adequately represent the total field on the outer boundary. The boundary condition imposed on the wave function in the process of deriving these interior solutions, via the FD/FEM method, is that the total field u equals $e^{jn\phi}, n = 0, 1, 2, \ldots N$. The interior solution can be represented on the outer boundary as a weighted sum of the boundary functions $e^{jn\phi}$ with the weight coefficients yet to be determined.

To this end, we represent the scattered field in the exterior region in terms of a finite series of outgoing cylindrical wave functions. Finally, the continuity conditions on the field and its derivative are enforced at the artificial boundary, resulting in a matrix equation of the order $4N \times 4N$ whose solution leads to the determination of the weight coefficients.

As mentioned earlier, for a scatterer of characteristic dimension ka, on the order of N harmonics are needed for the solution to be accurately represented, implying that N boundary functions should be employed at the artificial boundary in the Unimoment method. Suppose, however, that we generate an initial solution by applying the second-order $\mathcal{B}_2$ operator at Γ_2, where Γ_2 barely encloses the scatterer. Then, from the behavior of γ_n's investigated above, we know that the lower-order harmonic contents of this solution will be accurate and only the higher-order harmonics will require correction. This suggests that we can improve the ABC solution by following a Unimoment type of procedure, but by applying it to only a small fraction of the total number of harmonics needed to represent the scattered field at the outer boundary. This not only reduces the time it takes to generate the matrices representing the continuity equations applied at Γ_2, because of the reduction in the size of this matrix to a fraction of that in the Unimoment method, but it also reduces the matrix storage and solution time. Both of these are important factors in determining the feasibility of solving large-body scattering problems.

Strictly speaking, the procedure outlined above is based on the premise that there exists little or no coupling between the higher-order

harmonics that are being modified and the lower-order harmonics that are being left intact once they have been generated via the application of the ABC. We recall that for the canonical problem of the cylinder there was absolutely no coupling between the various harmonics. However, for a general scatterer, the harmonics do couple to each other, in the sense that a single harmonic in the incident field can produce all the harmonics in the scattered field. Fortunately, numerical experiments performed on different scatterer geometries have shown that this coupling between the harmonics, introduced by the arbitrary shape of the scatterer, is confined only to the adjacent harmonics, i.e., it is very much of the near-neighbor type. Furthermore, the coupling is even weaker between the propagating and the evanescent harmonics. As a result, to improve the ABC solution it is usually adequate to consider only a few, say about 10 harmonics for a body with a ka size of 50, with some of the harmonics falling in the transition region and the rest being evanescent. One suppresses the incoming portions of the scattered field for these harmonics while simultaneously adjusting their outgoing parts, by solving a 40×40 matrix equation (the size of the matrix is 4 times the number of harmonics), which neglects their coupling to the lower-order harmonics that have presumably been calculated sufficiently accurately using the second-order boundary operator. The realization of time saving in this approach, vis-a-vis the conventional Unimoment method, results from two factors. First, the number of times the interior problem needs to be solved is only a fraction of that in the Unimoment method; and, second, the matrix equation that corresponds to the continuity condition is also smaller by the same reduction ratio. It is also important to recognize that if one attempted to derive the solution strictly using the ABC, the outer boundary would have to be moved outward to a radius of about 2 to 3 ka, or even higher, and consequently, the number of mesh points would increase substantially, as would the computation time and the storage requirement. Figure 14 shows the effect of correcting for the harmonics $n = 40$ to 60 in the scattered field for the TE scattering from the 8λ cylinder. The corrected solution is seen to agree very well with the exact solution.

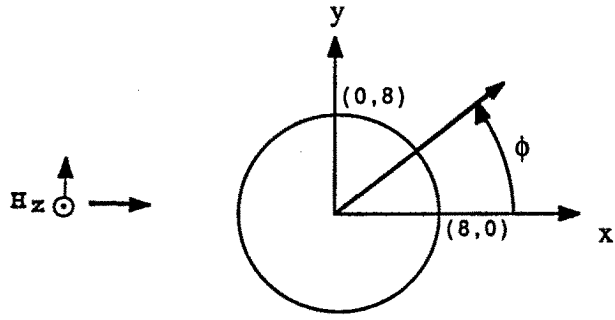

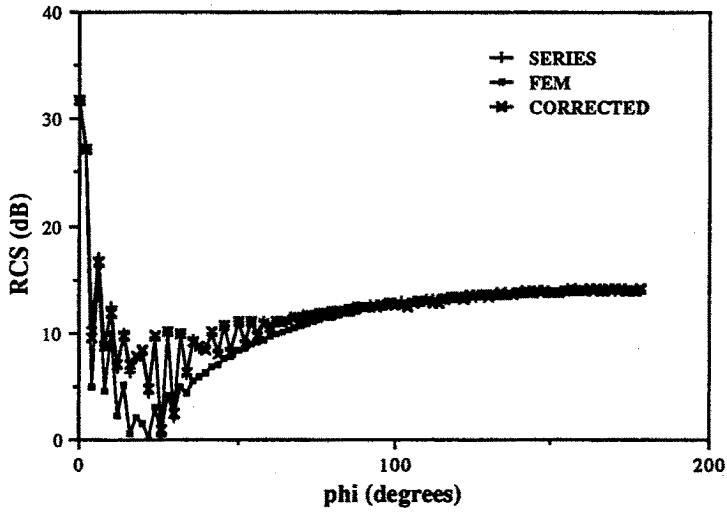

Figure 14 Effect of correcting for the harmonics n=40 through 60 in the Finite Element ABC solution for a conducting cylinder of radius 8λ, TE case, with B_2 applied at 8.2λ.

4.7 ABC for 3-D Scalar and Vector Fields

As shown in the Appendix, the 3-D counterpart of the scalar and vector absorbing boundary conditions can be derived by using recursion relations for the coefficients of the inverse powers of r in the asymptotic representation given by Wilcox. One could either choose to use these

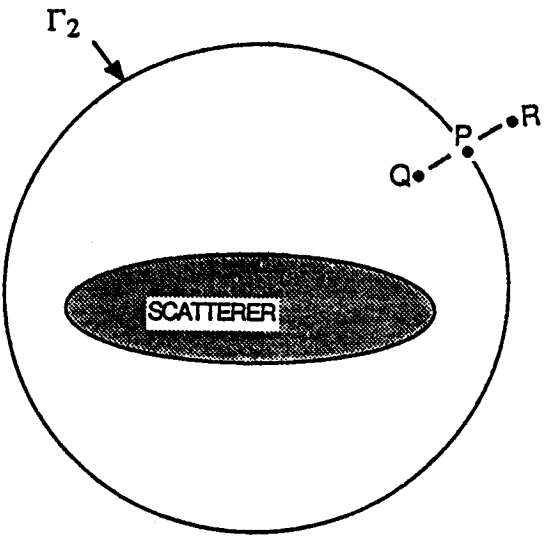

Figure 15 Geometry Pertaining to 3-D ABC.

boundary conditions to truncate the mesh at the outer boundary and use the 3-D version of the weak form given in (41) in the context of FEM, or employ a direct procedure outlined below that serves the same purpose.

Consider the point P on the outer boundary Γ_2, and the points R and Q lying just outside and inside the boundary, respectively, on the same radial line as shown in Fig. 15. In the Finite Difference method, we can truncate the mesh at Γ_2 provided we can write the field value at the point R by first expressing it in terms of the radial derivative of the field at P and then trading this derivative for the angular derivatives at P by using, say, a vector form of ABC. Alternatively, we can achieve the same goal by expressing the field value at R in terms of the values at P and Q, lying on the same radial line, via extrapolation as follows. We first use the two-term Wilcox representation

$$E(r) = \frac{e^{-jkr}}{r}\left[E_0(\theta,\phi) + E_1(\theta,\phi)\frac{1}{r}\right] \tag{46}$$

and solve for the two coefficients E_0 and E_1 appearing inside the brackets of the above equation, in terms of the field values of E at Q and P. This allows us to express the field value at R using (46) and enables us

to truncate the mesh at Γ_2. Note that no explicit angular derivatives are needed in this procedure, although they do get implicitly involved through the radial derivatives via the wave equation satisfied by the fields.

The procedure described above can be generalized to the case where the points P, Q, R do not all lie on a radial line. However, the angular derivatives are explicitly needed in this situation.

Numerical study of this approach for truncating the FD mesh in a region surrounding a scatterer for a 3-D vector scattering problem has been carried out successfully [16] in connection with the body of revolution (BOR) problem. Taking advantage of the azimuthal symmetry of this geometry, a modified form of the coupled azimuthal potentials (CAP's) introduced by Morgan, Chang, and Mei [10] can be used to solve the vector BOR problem. Specifically, the potentials are $u_m(r,\theta)$ and $v_m(r,\theta)$, where

$$E_\phi(r,\theta,\phi) = \sum_{m=-\infty}^{\infty} u_m(r,\theta)e^{jm\phi} \tag{47}$$

$$\eta_0 H_\phi(r,\theta,\phi) = \sum_{m=-\infty}^{\infty} v_m(r,\theta)e^{jm\phi} \tag{48}$$

Note that these potentials have the advantage of being continuous across dielectric interfaces, whereas the Debye potentials, typically used to solve the sphere problem, do not enjoy the same feature. It can be shown (for details see Chapters 2 and 6) that u_m and v_m satisfy the following coupled differential equations

$$\begin{aligned} A_1 u_m + B_1 \frac{\partial u_m}{\partial r} + C_1 \frac{\partial u_m}{\partial \theta} + D_1 \frac{\partial^2 u_m}{\partial r^2} + E_1 \frac{\partial^2 u_m}{\partial \theta^2} \\ + F_1 v_m + G_1 \frac{\partial v_m}{\partial r} + H_1 \frac{\partial v_m}{\partial \theta} = 0 \end{aligned} \tag{49}$$

$$\begin{aligned} A_2 v_m + B_2 \frac{\partial v_m}{\partial r} + C_2 \frac{\partial v_m}{\partial \theta} + D_2 \frac{\partial^2 v_m}{\partial r^2} + E_2 \frac{\partial^2 v_m}{\partial \theta^2} \\ + F_2 u_m + G_2 \frac{\partial u_m}{\partial r} + H_2 \frac{\partial u_m}{\partial \theta} = 0 \end{aligned} \tag{50}$$

where $A_1, \ldots H_1, A_2, \ldots, H_2$ are known functions of $m, r, \theta, \epsilon_r(r,\theta)$, and $\mu_r(r,\theta)$.

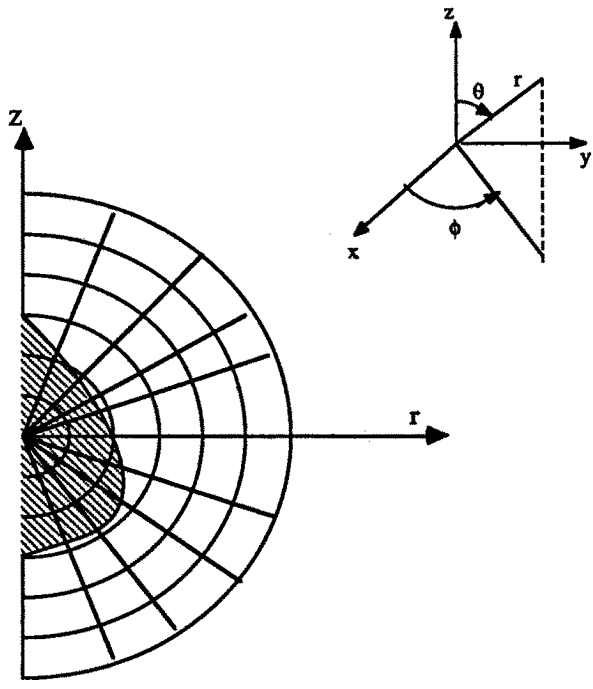

Figure 16 Geometry of the body of revolution problem showing the finite difference grid.

Next, consider a finite difference formulation in which a mesh consisting of nodes distributed along lines of constant r and constant θ is used (see Fig. 16.)

The above two equations are enforced at each interior point of the mesh. For those nodes on the outer boundary, the usual finite difference approximation to $\partial/\partial r$ and $\partial^2/\partial r^2$ cannot be used because of truncation. However, from the Wilcox expansion for the scattered fields, we see that u_m and v_m satisfy the following

$$u_m(r,\theta) = \frac{e^{-jkr}}{r}\left[A_{0m}(\theta) + \frac{A_{1m}(\theta)}{r} + \frac{A_{2m}(\theta)}{r^2} + \ldots\right] \tag{51}$$

$$v_m(r,\theta) = \frac{e^{-jkr}}{r}\left[B_{0m}(\theta) + \frac{B_{1m}(\theta)}{r} + \frac{B_{2m}(\theta)}{r^2} + \ldots\right] \tag{52}$$

If the outer boundary is sufficiently far from the scatterer, the terms of order $(1/r)^2$ and higher make a negligible contribution. Thus, under this approximation, we have:

$$u_m(r,\theta) = \frac{e^{-jkr}}{r}\left[A_{0m}(\theta) + \frac{A_{1m}(\theta)}{r}\right] \tag{53}$$

$$v_m(r,\theta) = \frac{e^{-jkr}}{r}\left[B_{0m}(\theta) + \frac{B_{1m}(\theta)}{r}\right] \tag{54}$$

We can now solve A_{0m}, A_{1m}, B_{0m}, and B_{1m} along a radial line, i.e., say $\theta = \theta_p$, in terms of the nodal values of u_m and v_m at P and Q (see Fig. 15). Once we have done this, we can substitute back into the two-term expansions to find the values of u_m and v_m at $\theta = \theta_p$ for any $r > r_p$. Thus, we can now find the needed expressions for $\partial u_m/\partial r, \partial^2 u_m/\partial r^2, \partial v_m/\partial r$, and $\partial^2 v_m/\partial r^2$ at node P in order to enforce the two coupled partial differential equations at this boundary node. It is worthwhile noting that no explicit absorbing boundary conditions in terms of the normal and angular derivatives are needed in this procedure, as they are in the approaches discussed earlier.

The above procedure has been used to investigate the problem of scattering by different shape BOR's including p.e.c. spheres of various sizes [16]. Good results have been obtained using meshes with outer boundary as close to the scatterer as $r = 1.4a$, or even less, where a is the radius of the sphere.

Next, we present some representative numerical results for the sphere, together with comparisons with the exact series solutions. The numerical values have been obtained using an outer radius which is 1.4 times the radius of the spheres. Figures 17 through 19 exhibit the results for a p.e.c. sphere of radius a where ka=16.0. The incident field is z-polarized and traveling in the negative x-direction. Figure 17 is a plot of both the calculated and the analytical values for the magnitude of J_θ, the transverse component of the current induced on the surface of the sphere in the plane $\phi = 0°$. The two results are seen to compare quite favorably with each other. In Figs. 18 and 19 we present the plots of the magnitude and phase , respectively, of the radial variation of the scattered H_ϕ as a function of the normalized distance from the surface of the sphere in the plane $\phi = 0°$ and in the direction $\theta = 90°$. This plot illustrates the fact that the scattered field does indeed begin to exhibit an outward traveling wave behavior

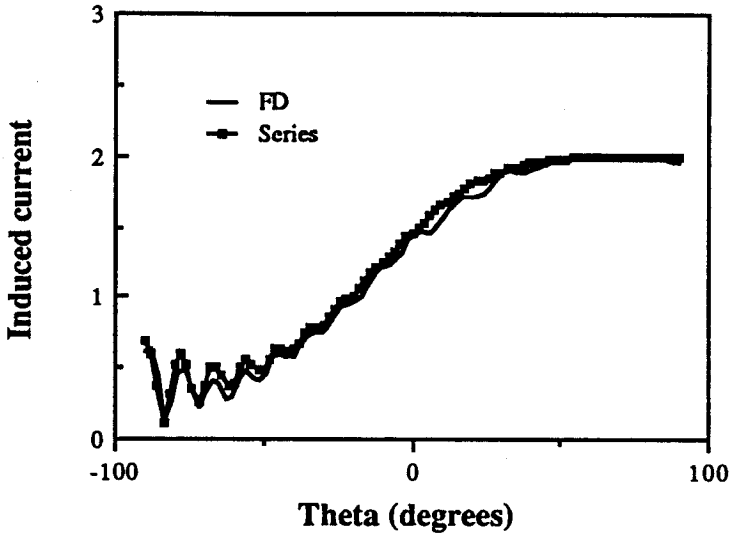

Figure 17 Transverse component of the induced current J_θ on a sphere vs. θ, in the plane $\phi = 0°$.

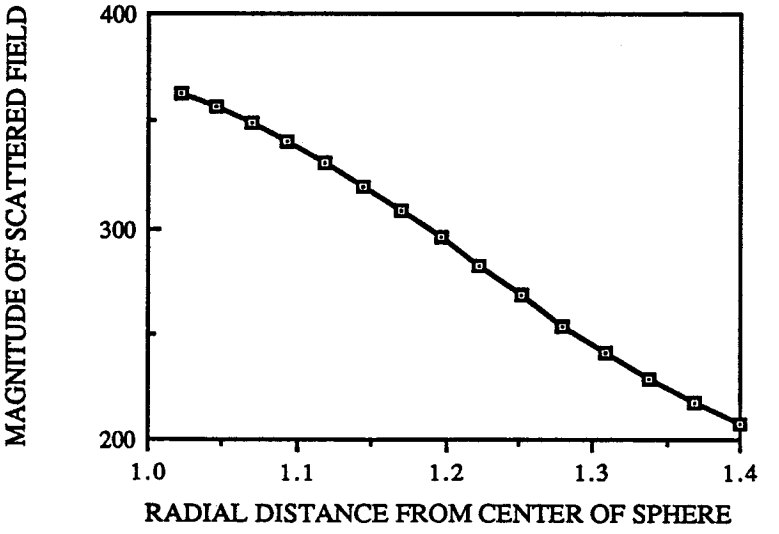

Figure 18 Magnitude of the scattered field, H_ϕ, vs. normalized radial distance in the plane, $\phi = 0°$, at $\theta = 90°$.

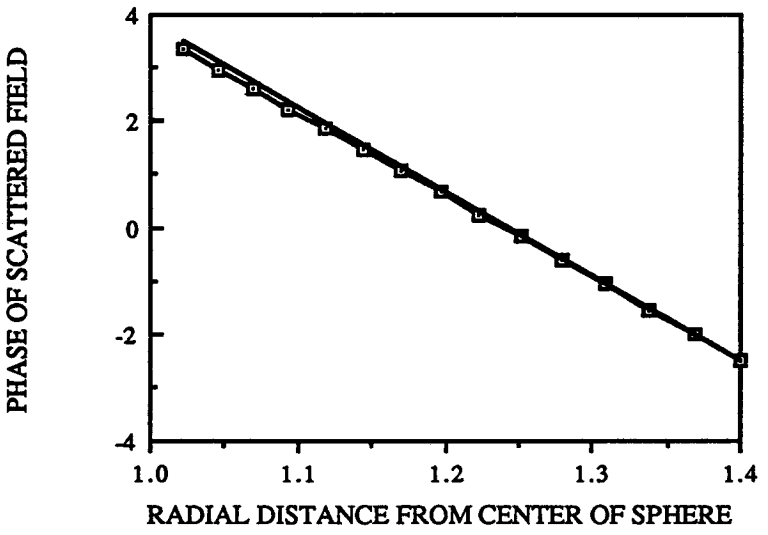

Figure 19 Phase of the scattered field, H_ϕ, vs. normalized radial distance in the plane, $\phi = 0°$, at $\theta = 90°$ (-□-), and the phase of a traveling wave field with $\exp(-\jmath kr)$ variation (—).

of the type $(e^{-\jmath kr})/r$, assumed in the asymptotic representation, even at distances not far from the surface of the sphere. In Fig. 19, the top plot is that of the phase of the function $e^{-\jmath kr}$ and it is evident that the the phase variation of the calculated value of the scattered H field indeed exhibits a similar behavior.

Appendix:

Derivation of ABC's Using Recursion Relations

a. *2-D Absorbing Boundary Condition*

In this appendix, we present an alternative derivation of the absorbing boundary condition, based on the use of recursion relationships satisfied by the coefficients $a_n(\phi)$ in the Wilcox expansion, which is repeated below for convenience

$$u(\rho,\phi) = \frac{e^{-\jmath k\rho}}{\rho^{1/2}} \sum_{n=0}^{\infty} \frac{a_n(\phi)}{\rho^n} \tag{A1}$$

Imposing the requirement that $u(\rho,\phi)$ satisfy the wave equation $\nabla^2 u + k^2 u = 0$, one can readily derive the recursion relationship

$$-2\jmath k\,(n+1)\,a_{n+1} = (n+\tfrac{1}{2})^2\,a_n + D\,a_n \tag{A2}$$

where $D = \partial^2/\partial\phi^2$.

Next, we use (A1) to express the radial derivative uf u, i.e. u_ρ, as

$$\begin{aligned} u_\rho &= -\jmath k\,u - \frac{e^{-\jmath k\rho}}{\rho^{3/2}} \sum_{n=0}^{\infty} \frac{(n+\frac{1}{2})\,a_n}{\rho^n} \\ &= \left(-\jmath k - \frac{1}{2\rho}\right) u - \frac{e^{-\jmath k\rho}}{\rho^{5/2}} \sum_{n=1}^{\infty} \frac{n a_n}{\rho^{n-1}} \end{aligned} \tag{A3}$$

Replacing na_n in the summation in A3 using A2, we get

$$\begin{aligned} u_\rho = &\left(-\jmath k - \frac{1}{2\rho} + \frac{1}{8\jmath k\rho^2}\right) u \\ &+ \frac{1}{2\jmath k\rho^2} Du + \frac{e^{-\jmath k\rho}}{\jmath k\rho^{7/2}} \sum_{n=1}^{\infty} \frac{n a_n}{\rho^{n-1}} + O\left(\frac{1}{\rho^{9/2}}\right) \end{aligned} \tag{A4}$$

Once again, replacing na_n in (A4) and using the recursion relation, we get

$$\begin{aligned} u_\rho = &\left(-\jmath k - \frac{1}{2\rho} + \frac{1}{8\jmath k\rho^2} + \frac{1}{8k^2\rho^3}\right) u \\ &+ \left(\frac{1}{2\jmath k\rho^2} + \frac{1}{2k^2\rho^3}\right) Du + O\left(\frac{1}{\rho^{9/2}}\right) \\ = &\,\alpha(\rho)\,u + \beta(\rho)\,u_{\phi\phi} \end{aligned} \tag{A5}$$

Equation (A5) is seen to be identical to (12) with $\alpha(\rho)$ and $\beta(\rho)$ given by (22) and (23).

b. 3-D Scalar Absorbing Boundary Condition

We present below, for reference, the outline of the derivation of the three-dimensional scalar boundary conditions. For details the reader is referred to [10].

Let $u(r,\theta,\phi)$ satisfy the scalar wave equation

$$\nabla^2 u + k^2 u = 0 \tag{A6}$$

and be expressed asymptotically as

$$u = \frac{e^{-\jmath kr}}{r} \sum_{n=0}^{\infty} \frac{a_n(\theta,\phi)}{r^n} \tag{A7}$$

Then it can be shown that the a_n satisfy the recursion relationship

$$-2\jmath k\, n a_n = n(n-1)\, a_{n-1} + D a_{n-1} \tag{A8}$$

Using (A7) to write u_r, and incorporating the recursion relationship repeatedly in the resulting expression, yields the following compact form for u_r, after a slight rearrangement

$$u_r = -\jmath k\{\alpha(r)\, u + \beta(r)\, Du\} \tag{A9}$$

where D = Beltrami's operator and Df is given by

$$Df = \frac{1}{\sin\theta}\frac{\partial}{\partial\theta}\left(\sin\theta\frac{\partial f}{\partial\theta}\right) + \frac{1}{\sin^2\theta}\frac{\partial^2 f}{\partial\phi^2} \tag{A10a}$$

and

$$\alpha(r) = (1 + \frac{1}{\jmath kr}); \quad \beta(r) = \frac{1}{2(kr)^2\alpha(r)} \tag{A10b}$$

up to and including terms of order r^{-4}.

Equation (A9) is the desired representation for the 3-D ABC for a scalar u.

c. 3-D Vector Boundary Condition

For a 3-D vector field $\overline{E}$ (or $\overline{H}$) one can follow exactly the same procedure as in the previous section of this appendix, to express $\hat{r} \times \nabla \times \overline{E}$ in terms of E and its angular derivatives. Only a thumbnail

sketch of the derivation is presented here and the reader is referred to [16] for further details.

The first step is to use the Wilcox representation

$$\overline{E} = \frac{e^{-jkr}}{r} \sum_{n=0}^{\infty} \frac{\overline{A}_n(\theta,\phi)}{r^n} \tag{A11}$$

From (A11), we can get

$$\nabla \times \overline{E} = \left\{ -jk\,\hat{r} \times -\frac{(1+D_1)}{r} \right\} \overline{E} - \frac{e^{-jkr}}{r^2} \sum_{n=1}^{\infty} \frac{n\overline{A}_{nt}}{r^n} \tag{A12}$$

where $\overline{A}_{nt} = \hat{r} \times \overline{A}_n$, is the transverse component of $\overline{A}_n$ and, for the vector $\overline{F}$, $D_1\overline{F}$ is given by

$$D_1\overline{F} = \frac{1}{\sin\theta} \left[\frac{\partial}{\partial\theta}(\sin\theta F^{\phi}) - \frac{\partial F^{\theta}}{\partial\theta} \right] \hat{r}$$

$$+ \frac{1}{\sin\theta} \left[\frac{\partial F^{r}}{\partial\theta} - \sin\theta\, F^{\phi} \right] \hat{\theta} + \left[F^{\theta} - \frac{\partial F^{r}}{\partial\theta} \right] \hat{\phi}$$

Using the recursion relation

$$-2jk\,n\overline{A}_{nt} = n(n-1)(\overline{A}_{n-1})_t + D_4\,\overline{A}_{n-1} \tag{A13}$$

where

$$D_4\,\overline{A}_n = (DA_n^{\theta} + D_{\theta}\,\overline{A}_n)\,\hat{\theta} + (DA_n^{\phi} + D_{\phi}\,\overline{A}_n)\,\hat{\theta}$$

$$D_{\theta}\,\overline{A}_n = 2\frac{\partial A_n^{r}}{\partial\theta} - \frac{1}{\sin^2\theta} A_n^{\theta} - \frac{2\cos\theta}{\sin^2\theta}\frac{\partial A_n^{\phi}}{\partial\phi} \tag{A14}$$

$$D_{\phi}\,\overline{A}_n = \frac{2}{\sin\theta}\frac{\partial A_n^{r}}{\partial\phi} + \frac{2\cos\theta}{\sin^2\theta}\frac{\partial A_n^{\theta}}{\partial\phi} - \frac{1}{\sin^2\theta} A_n^{\phi}$$

and D is Beltrami's operator, we can once again derive the representation, correct to r^{-4}.

$$\nabla \times \overline{E} = \overline{\alpha}(r)\,\overline{E} + \beta(r)\,D_4\,\overline{E} \tag{A15}$$

where

$$\overline{\alpha}(r) = -\jmath k\left(\hat{r} \times \left(1 + \frac{1}{\jmath kr}\right) - \frac{D_1}{\jmath kr}\right) \tag{A16}$$

and

$$\beta(r) = \frac{1}{2\jmath kr^2}\frac{1}{(1 + 1/\jmath kr)} \tag{A17}$$

Equation (A15) is the desired relationship for the vector ABC.

Acknowledgements

The authors are pleased to acknowledge many helpful discussions with Prof. A. F. Peterson, and Messrs. Rick Gordon, Ahmed Khebir, and Ammar Kouki of the Electromagnetic Communication Laboratory at the University of Illinois. We are especially thankful to Rick Gordon for his contributions to section 4.7 and to the material presented in the Appendix.

This work was supported in part by the Joint Services Electronics Program under Grant #N00014-84-C-0149.

References

[1] McDonald, B. H., and A. Wexler, "Finite element solution of unbounded field problems," *IEEE Trans. Microwave Theory Tech.*, **MTT-20**, 841–847, 1972.

[2] Engquist, B., and A. Majda, "Radiation boundary conditions for the numerical simulation of waves," *Math. Comp.*, **31**, 629–651, 1977.

[3] MacCamy, R., and S. Marin, "A finite element method for exterior interface problems," *Int. J. Math. & Math. Sci.*, **3**, 311–350, 1980.

[4] Kriegsmann, G. A., and C. S. Morawetz, "Solving the Helmholtz equation for exterior problems with variable index of refraction: I," *SIAM J. Sci. Stat.*, **1**, 371–385, 1980.

[5] Bayliss, A., M. Gunzburger, and E. Turkel, "Boundary conditions for the numerical solution of elliptic equations in exterior regions," *SIAM J. Appl. Math.*, **42**, 430–451, 1982.

[6] Meltz, G., B. J. McCartin, and L. J. Bahrmasel, "Application of the control region approximation to electromagnetic scattering," *URSI Radio Science Meeting Program and Abstracts*, p. 185, Blacksburg, Virginia, June 1987. Also, see Chapter 5 of this book.

[7] Mei, K. K., "Unimoment method of solving antenna and scattering problem," *IEEE Trans. Antennas Propagat.*, **AP-22**, 760–766, 1974.

[8] Chang, S. K., and K. K. Mei, "Application of the unimoment method to electromagnetic scattering of dielectric cylinders," *IEEE Trans. Antennas Propagat.*, **AP-24**, 34–42, 1976.

[9] Morgan, M. A., and K. K. Mei, "Finite-element computation of scattering by inhomogeneous penetrable bodies of revolution," *IEEE Trans. Antennas Propagat.*, **AP-27**, 202–214, 1979.

[10] Morgan, M. A., S. K. Chang, and K. K. Mei, "Coupled azimuthal potentials for electromagnetic field problems in inhomogeneous axially symmetric media," *IEEE Trans. Antennas Propagat*, **AP-25**, 413–417, 1977

[11] Wilcox, C. H., "An expansion theorem for electromagnetic fields," *Comm. Pure & Appl. Math.*, **9**, 115–134, 1956.

[12] Kriegsmann, G. A., A. Taflove, and K. R. Umashankar, "A new formulation of electromagnetic wave scattering using an on-surface radiation boundary condition approach," *IEEE Trans. Antennas Propagat.*, **AP-35**, 153–161, 1987. Also, see Chapter 8.

[13] Silvester, P., and R. L. Ferrari, *Finite Elements for Electrical Engineers*. Cambridge, U.K. : Cambridge University Press, 1983

[14] Strang, G. and G. J. Fix, *An Analysis of the Finite Element Method*. Englewood Cliffs, N.J. : Prentice-Hall, Inc., 1973.

[15] Reddy, J. N., *An Introduction to the Finite-Element Method*. New York, N.Y. : McGraw-Hill, 1984.

[16] Mittra, R., and R. Gordon, "Radar scattering from bodies of revolution using an efficient partial differential equation algorithm," Submitted to *IEEE Trans. Antennas Propagat.*